Accepted Manuscript

Chemosphere

Sea salt sodium record from Talos Dome (East Antarctica) as a potential proxy of the Antarctic past sea ice extent

M. Severi, S. Becagli, L. Caiazzo, V. Ciardini, E. Colizza, F. Giardi, K. Mezgec, C. Scarchilli, B. Stenni, E.R. Thomas, R. Traversi, R. Udisti

Highlights

- Sea salt sodium at Talos Dome can be used as a reliable proxy of sea ice extent.

- A positive relationship between $ssNa^+$ flux and SIE maxima was found.

- SIE of the Ross Sea and Western Pacific was reconstructed over the 20th century

- SIE variability increased starting from 1990s.

1 **Sea salt sodium record from Talos Dome (East Antarctica) as a potential proxy**

2 **of the Antarctic past sea ice extent.**

3

4 **M. Severi [1]*, S. Becagli [1], L. Caiazzo [1], V. Ciardini [2], E. Colizza [3], F. Giardi [1], K. Mezgec [3], C.**

5 **Scarchilli [2], B. Stenni [4], E.R. Thomas [5], R. Traversi [1] and R. Udisti [1,6].**

6

7 [1] University of Florence, Chemistry Dept. "Ugo Schiff", Via della Lastruccia, 3 – 50019, Sesto

8 Fiorentino (FI) – Italy.

9 [2] Laboratory for Earth Observations and Analyses, ENEA, Rome, Italy.

10 [3] Department of Mathematics and Geosciences, University of Trieste, Trieste, Italy.

11 [4] Department of Environmental Sciences, Informatics and Statistics, "Ca' Foscari" University of

12 Venice, Italy.

13 [5] British Antarctic Survey, Cambridge, UK

14 [6] ISAC CNR, Via Gobetti 101, 40129, Bologna, Italy

15

16 *Corresponding author: Mirko Severi, e-mail address: mirko.severi@unifi.it, tel: +39 055 457 3287

17

18 **Abstract**

19 Antarctic sea ice has shown an increasing trend in recent decades, but with strong regional

20 differences from one sector to another of the Southern Ocean. The Ross Sea and the Indian sectors

21 have seen an increase in sea ice during the satellite era (1979 onwards). Here we present a record of

22 $ssNa^+$ flux in the Talos Dome region during a 25-year period spanning from 1979 to 2003, showing

23 that this marker could be used as a potential proxy for reconstructing the sea ice extent in the Ross

24 Sea and Western Pacific Ocean at least for recent decades. After finding a positive relationship

25 between the maxima in sea ice extent for a 25-year period, we used this relationship in the

26 TALDICE record in order to reconstruct the sea ice conditions over the 20th century. Our tentative

27 reconstruction highlighted a decline in the sea ice extent (SIE) starting in the 1950s and pointed out

28 a higher variability of SIE starting from the 1960s and that the largest sea ice extents of the last

29 century occurred during the 1990s.

30

31 **Keywords**

32 Sea-ice, ice-core, Antarctica, paleo reconstruction, climate change, Ross Sea.

33

34 **1. Introduction**

35 Sea-ice represents a powerful phenomenon exerting a strong influence on the oceanic, biological

36 and climatic systems and, given its importance, it is a focus in environmental research. The

37 expansion and retreat of Antarctic sea-ice is one of the most striking seasonal changes affecting the

38 Earth today, effectively increasing by two fold the surface area of Antarctica (Allen et al., 2011).

39 Sea-ice plays a key role in the production and upkeep of deep waters in the ocean and therefore in

40 the whole global ocean circulation system (Dieckmann and Hellmer, 2010). Moreover, sea-ice

41 greatly affects the transfer of energy at the ocean-atmosphere interface as it shows a much higher

42 albedo with respect to open water (Brandt et al., 2005) and is thus able to reflect more incoming

43 radiation deeply changing the radiative balance. The presence of sea-ice also represents a physical

44 barrier that successfully inhibits the transfer of heat, moisture and trace gases (such as CO_2)

45 between the ocean and the atmosphere (Bopp et al., 2003). Additionally sea-ice has a direct

46 influence on the Antarctic biota and it has been suggested that it is linked to the "biological pump"

47 and thus to the global carbon cycle (Sarmiento and Gruber, 2006).

48 For all these reasons, despite an unknown exact mechanism, sea-ice plays a critical role in the polar

49 amplification of climate change (Serreze and Barry, 2011) and, therefore, it is important to predict

50 changes in sea ice under the future conditions of an ongoing climate change. A better understanding

51 of the links between sea-ice and climate and a real improvement of the models require a large series

52 of long observational datasets. Unfortunately, satellite observations only began in the 1970s and

53 before that we rely on sporadic observations and proxy data. (Abram et al., 2013).

54 The reconstructions of Antarctic sea-ice cover used as data for the parameterization of models have

55 been so far mainly based on diatom remains found in marine sediment cores (Armand et al., 2005;

56 Armand et al., 2008). These diatom based reconstructions can provide quantitative estimates of

57 yearly sea-ice presence and/or duration and can allow us to draw limits for winter and summer sea-

58 ice extents (Esper and Gersonde, 2014). Particularly large datasets have been made available based

59 on the occurrence of sea-ice related diatoms (Gersonde at al., 2005) and, in the last years, new

60 methods based on a sea-ice biomarker known as IP_{25} have been developed (Belt et al., 2007; Belt

61 and Muller, 2013) in order to reconstruct the Arctic sea-ice cover in the past. In more recent years,

62 the analysis of an organic geochemical lipid biomarker, called $IPSO_{25}$, has been proposed as a

63 possible proxy measure of Antarctic sea ice (Masse et al., 2011; Collins et al., 2013).

64 Ice cores drilled in the Antarctic ice-sheet represent a very different kind of proxy record with

65 respect to ocean sediment cores. The information about sea-ice is present in the ice cores only if it is

66 transported from the surface of the ocean to the atmosphere. The information about sea ice is

67 transported from the surface of the ocean to the atmosphere and unlike the sediment records is

68 representative of sea ice in a particular sector, rather a single site. One of the greatest advantages of

69 using ice cores to reconstruct sea-ice variations is their higher temporal resolution with respect to

70 marine sediment cores. Reconstruction of sea-ice from ice-core proxies have so far been based on

71 concentrations or fluxes of sodium, methanesulphonic acid (MSA, $CH_3SO_3^-$) and, more recently,

72 halogen species.

73 Sea salt sodium ($ssNa^+$) has been used to quantify sea-ice variations (Wolff et al., 2006) based on

74 the formation of high salinity "frost flowers" and brine (Rankin et al., 2000) on sea ice surfaces.

75 However, a recent laboratory experiment (Roscoe et al., 2011) shows that frost flowers are very

76 stable also in the presence of wind and no significant aerosol emission was observed. For this

77 reason, such source of $ssNa^+$ is difficult to distinguish from other dominating sources, such as sea

78   spray aerosol, which has been proved to be dominant at many drilling sites, e.g. James Ross Island

79   (Abram et al., 2011) and Law Dome (Curran et al., 1998). Yang et al. (2008) proposed more

80   recently that a massive source of Na^+ in several Antarctic drilling sites could be represented by

81   "blowing snow", i.e. the snow lying on sea ice, rich in salts, that can be easily lifted into the air

82   through blowing-snow events. Levine et al. (2014) found in their model experiment that, on an

83   interannual scale, meteorology, and not sea ice extent, is the dominant control on the atmospheric

84   concentration of sea salt. Which is the real factor controlling the sea salt content in Antarctic sites is

85   so far still an open and debated question.

86   Methanesulphonic acid (MSA) was first used quantitatively for a reconstruction of sea ice extent

87   (SIE hereafter) by Curran et al. (2003) in an ice-core drilled at Law Dome. Afterwards this marker

88   has been largely investigated as a sea-ice proxy in several drilling sites (Abram et al., 2010; Becagli

89   et al., 2009; Becagli et al., 2016; Foster et al., 2006; Criscitiello et al., 2013) highlighting both

90   positive and negative relationship between MSA and sea ice. However, this compound is not

91   always fully stable in snow and ice and can be easily remobilised in the ice matrix after deposition

92   (Smith et al., 2004) limiting its utility for long-term sea ice reconstructions at certain sites.

93   Recently, two halogens, namely iodine and bromine, has been suggested as ice core proxies useful

94   to reconstruct the past sea ice concentration at Talos Dome (Spolaor et al., 2013) and at Law Dome

95   (Vallelonga et al., 2016); furthermore the Canadian Arctic sea ice was successfully reconstructed

96   for the last 120.000 years from the NEEM ice core (Greenland) using the bromine content as a

97   proxy (Spolaor et al. 2016).

98   In this paper we assess the suitability of ss-Na^+ at Talos Dome (TD here hence) as a proxy for past

99   sea ice conditions. The reliability of the sea salt sodium record from Talos Dome site in serving as a

100   potential proxy of SIE is supported by the comparison between the ssNa^+ stratigraphic profile and

101   the calculation of sea ice extent achieved by satellite data in the 1979-2003 time period.

102   Severi et al. (2009) showed already the relationship between Na^+ and SOI (Southern Oscillation

103   Index) and the good agreement between $nssSO_4^{2-}$ and MSA with the anomalies in SIE for the 1975-

104 1995 period suggesting the potential of this site in recording variations in sea ice and sea ice-related

105 parameters. The results obtained from the analysis of a 5.65 m snowpit give further support for the

106 use of ssNa$^+$ as qualitative sea-ice tracer at the TALDICE drilling site, where sea-spray deposition

107 and fractionation effects have been deeply investigated in the past (Becagli et al., 2004; Traversi et

108 al., 2004).

109

110 **2. Materials and Methods**

111 **2.1 Sampling site**

112 Talos Dome is a coastal dome (figure 1) in Northern Victoria Land on the edge of the East

113 Antarctic plateau and is located about 290 km from the Southern Ocean (Oates Land–George V

114 Land), 250 km from the Ross Sea, and 275 km from the Italian "Mario Zucchelli" Station (Terra
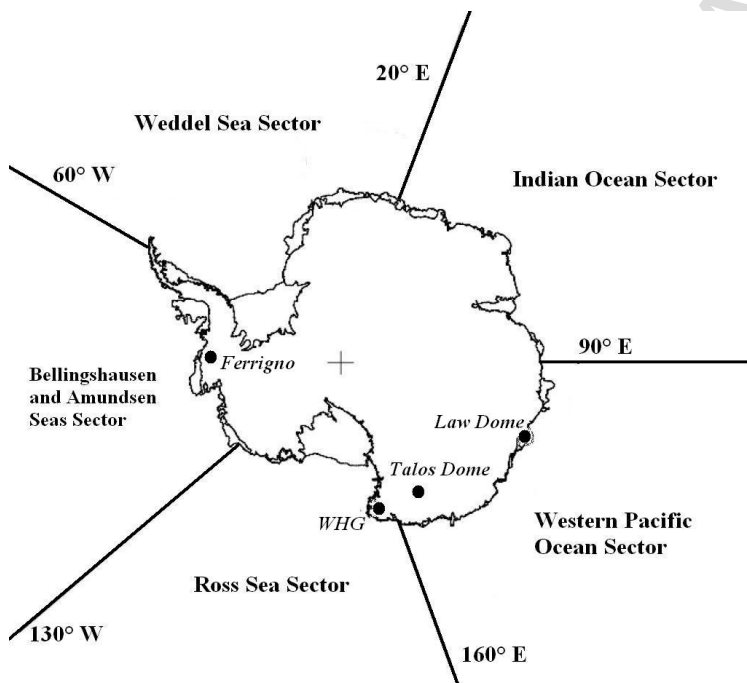
Figure 1. Map of the Antarctic continent showing Talos Dome, Law Dome, Ferrigno and Whitehall Glacier sites and the division in five sectors of the Southern Ocean as in Cavalieri and Parkinson (2008).

115 Nova Bay). The site chosen for digging a snow-pit (159° 10' 30.9'' E, 72° 49' 04.6'' S, 2330 m a.s.l.)

116 was close to the centre of the dome and also to the TALDICE deep drilling site (Stenni et al., 2011;

117 Severi et al., 2012).

5

118 During the 2003/2004 Antarctic campaign a snow pit was dug by hand to a depth of 565 cm and

119 more than 200 samples were continuously collected along a vertical line using pre-cleaned PET

120 vials with a mean resolution of 2.5 cm, wearing sterile overalls and gloves. All the samples were

121 then stored in sealed polyethylene bags and kept frozen in insulated boxes for the transport to Italy.

122

123 **2.2 Analysis method**

124 The samples were melted in a clean room under a class-100 laminar flow hood shortly before

125 chemical analysis. The method used for the analysis of the ionic content of the samples was based

126 on a fully automated ion chromatographic system described in details elsewhere (Caiazzo et al.

127 2016; Morganti et al., 2007; Severi et al., 2009).

128 Na^+ content in Antarctic aerosol, and thus snow and ice, is always dominated by sea salt, especially

129 in interglacial periods, showing a minor contribution of dust leachable Na^+. As an example, the

130 non-sea salt contribution to Na^+ total budget at Dome C during the Holocene was estimated to be

131 around 2% (Röthlisberger et al., 2002) and therefore Na^+ direct measurement could be reasonably

132 taken as a marker of sea salt. Nonetheless, the ''pure'' sea salt contribution can be more reliably

133 assessed if the mineral dust contribution to Na^+ content is cut off. Therefore, we corrected the total

134 Na^+ content using non sea-salt Ca^{2+} ($nssCa^{2+}$) as crustal marker and a simple two-variable, two-

135 equation system allowing the evaluation of the ss- and nss-fractions of both Na^+ and Ca^{2+}:

136 1) $ssNa^+ = totNa^+ - nssCa^{2+}/R_{crust}$

137 2) $nssCa^{2+} = Ca^{2+} - R_{sea\ water} * ssNa^+$

138 $(Ca^{2+}/Na^+ = 0.038 = R_{sea\ water})$ $(Ca^{2+}/Na^+ = 1.78 = R_{crust})$

139 where R_{crust} and $R_{sea\ water}$ are the mean ratio (w/w) in the Earth crust and in bulk seawater,

140 respectively (Bowen, 1979). For the TD site, on average only 5% of the total Na^+ does not come

141 from sea spray.

142 The snow pit was dated by annual layer counting, using a multi-parametric approach as described in

143 Severi et al. (2009). Using this kind of dating in our record, we cannot exclude misinterpretation in

144 the annual layers counting or missing years in the snow layers due to wind ablation of the snow

145 layers and low accumulation (Frezzotti et al., 2007). In order to minimize these type of errors we

146 smoothed our annual data with a 3-year running average, indeed we have to take into account a

147 possible dating error of 2/3 years.

148 In order to account for the dilution of the original atmospheric aerosol concentrations in the snow

149 pit samples by snow accumulation, the measured concentrations had to be corrected for this effect.

150 This was achieved by multiplying the measured concentrations by the accumulation rate at the

151 respective depth or age, resulting in the total deposition flux of the aerosol (Wolff et al., 2006). The

152 accumulation rate along the snow pit was calculated according to the age scale of Severi et

153 al.(2009) and to the density profile of the snow pit achieved using the method described in Severi et

154 al. (2009). Following this methodology the annual ssNa$^+$ flux was calculated by multiplying the

155 mean annual concentration values by the annual accumulation rates at the TD site.

156 An high resolution ssNa$^+$ flux time series for TD site, spanning the last century (2003-1920 DC),

157 was built by overlapping the TALDICE ice core Na$^+$ record and the snowpit data. The TALDICE

158 deep ice core started at a depth of 5.0 m and we used our high resolution (2.5 cm) snow pit data to

159 fill the missing top part of the core. The TALDICE Na$^+$ flux (at 4 cm resolution) was calculated

160 using the past accumulation rates modeled in the AICC2012 age scale (Bazin et al. 2012, Veres et

161 al., 2012) at 1 m resolution.

162

163 **2.3 Sea Ice Extent (SIE) data**

164 Time series of the monthly mean sea ice extent for each region of the Southern Ocean (Weddell

165 Sea, Indian Ocean, Western-Pacific Ocean, Ross Sea and Bellingshausen and Amundsen Seas)

166 spanning from November 1979 to December 2003, were calculated from observations of sea ice

167 concentrations from passive microwave satellite radiometers (Sea Ice Concentrations from Nimbus-

168 7 SMMR and DMSP SSM/I-SSMIS Passive Microwave Data) (Parkinson and Cavalieri, 2012).

169   Sea ice concentration is published at a regular 25 km resolution daily. The ice extent is calculated

170   by summing the areas of the pixels within each region with ice concentrations of at least 15% and

171   then averaged on a monthly basis.

172

173   **2.4 Back-Trajectories (TJ) air masses**

174   Three-day back trajectories were computed daily, arriving at 1000 m and 3000 m over TD at

175   12UTC. The backward trajectories were generated using the Hybrid Single-Particle Lagrangian

176   Integrated Trajectory (HYSPLIT) model developed by NOAA and Australia's Bureau of

177   Meteorology (Draxler and Rolph, 2012), for the period spanning from 1979 to 2003, covering

178   completely the snowpit time range. HYSPLIT is initialised with the European Centre for Medium

179   Range Weather Forecast (ECMWF) ERA Interim Reanalysis meteorological data fields (Simmons

180   et al., 2006) with a regular grid of 1°x1°. Errors in TJ calculations after 3 days are estimated in the

181   range 10 to 20% of the travel distance (Schlosser et al. (2008), Scarchilli et al. (2011)). The TJs

182   were projected onto the Sea Ice Cover (SIC) field, and the nearest model value was associated with

183   hourly SIC value along the trajectory path, assuming a constant ice cover condition during the day.

184

185   **2.5 Climatic Indexes**

186   Our analysis takes into account the Inter-decadal Pacific Oscillation (IPO) and the Antarctic

187   Oscillation (AAO), in order to better understand the possible linkage between SIE and ssNa$^+$ flux at

188   TD.

189   IPO is a naturally fluctuating atmospheric pressure which is responsible of warming or cooling of

190   sea surface temperature (SST) over the entire Pacific Basin. Each IPO cycle can last from 20 to 30

191   years (Salinger et al., 2001). Since the latest 1990s the IPO index has been in a "negative phase",

192   causing a decrease of SST and, as a consequence, sea ice to rapidly increase. In our analysis we

193   used the dataset available online at https://data.mfe.govt.nz/x/ReypdH.

194   The circulation variability of the lower atmosphere in the Southern Hemisphere is triggered by the

195   annular mode in the pressure field anomaly at various temporal time, from seasonal to inter-annual

196   (Thomson and Wallace, 2000). This mode has been referred to as the Antarctic Oscillation (AAO),

197   or the Southern Annular Mode (SAM) and it is significantly related to the strength of the westerlies

198   and storm track around Antarctica (Baldwin, 2001); we used the dataset described in Marshal

199   (2003) in order to discuss the relationship between SIE and ssNa$^+$ flux data.

200

201   **3. Results**

202   **Figure 2** shows the maximum values of SIE for two selected sectors of the Southern Ocean (Ross

203   Sea and Western Pacific Ocean) and for the total Antarctic continent in the time period spanning

204   from 1979 to 2003. On average, over this 25-year period, maximum SIE occurs in September for all

205   sectors; hence, we refer in our work to the SIE maxima as the September monthly average in each

206   year. For the total Antarctic sea ice, the SIE maxima range from a minimum of 17.7×10^6 km^2 in

207   1986 to a maximum of 18.9×10^6 km^2 in 1998. We applied a linear regression to the September

208   monthly average values for the Antarctic total SIE and for the two selected sectors of the Southern

209   Ocean (see bold lines in figure 2). The trend of the September Antarctic SIE shows a positive slope

210   in agreement with previous results (Parkinson and Cavalieri, 2012) confirming that in the studied

211   period there is a general trend to the increase of the SIE for the Southern hemisphere The SIE

212   maxima of the Western Pacific Ocean (90°E – 160°E) shows a slightly decreasing trend whereas

213   the Ross Sea sector (160°E – 130°W) shows a positive trend of the September SIE trend. In

214   summary we can assess that, while there is a general increase of SIE at continental scale in

215   Antarctica mostly driven by the Ross Sea sector, the variations of the SIE around the continent are

216   different from one sector to another of the Southern Ocean, showing both positive and negative

217   trends (Parkinson and Cavalieri, 2012; Jones et al., 2016).
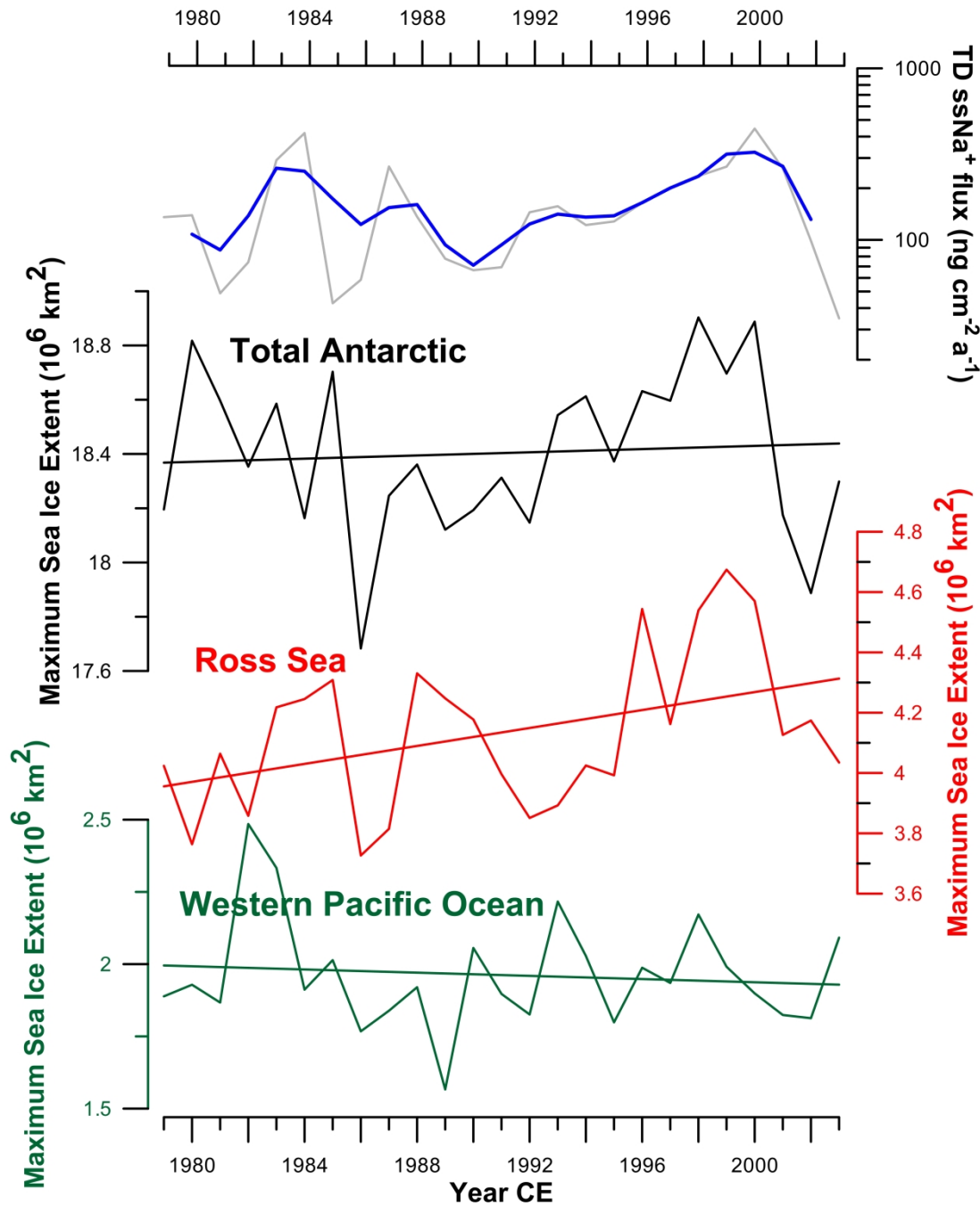
Figure 2. Maximum September Sea Ice Extent (calculated as monthly average) from 1979 to 2003 as reconstructed from satellite measurement for the Western Pacific Ocean (green) and the Ross Sea (red) sectors of the Southern Ocean. The total Antarctic SIE is shown as a black line and it is calculated as the sum of the five sectors shown in figure 1. For each sector the trend of the September SIE over the 25-year period is also shown as a solid line. The top panel shows the profile of the ssNa$^+$ flux at Talos Dome as yearly mean values (light grey line) and as three-year running mean (red line).

The top panel of figure 2 shows the ssNa$^+$ flux measured in the Talos Dome snow pit.. A simple 3-years running average is superposed in order to minimize dating errors due to low accumulation and post depositional phenomena. A general agreement with the maximum SIE of the whole continent is evident; for example there is an increase both in the ssNa$^+$ flux and in the SIE starting from the

224 beginning of the 1990's. The comparison with the SIE of each sector of the Southern Ocean shows

225 less evident common features even if some similarities between ssNa$^+$ flux and maximum SIE

226 appear for the Ross Sea sector.
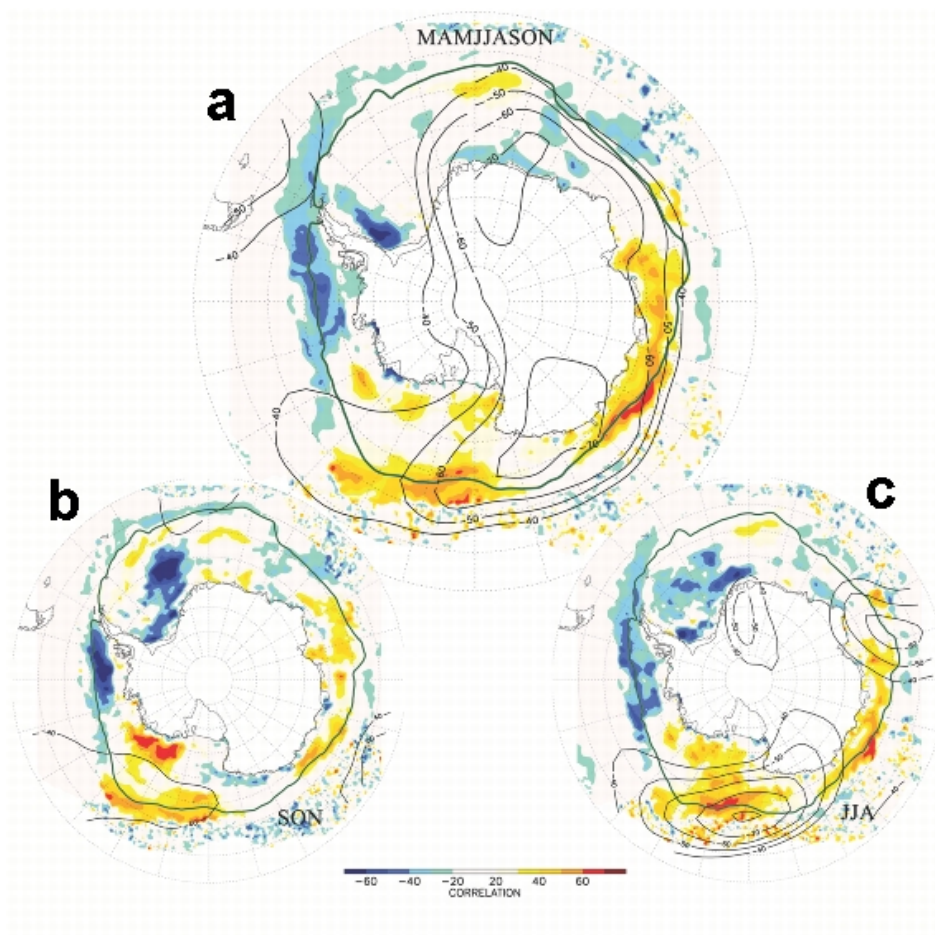
227

Figure 3. Spatial correlation between 3 year running averaged ssNa+ from TD snow pit and 3 year running averaged Sea Ice Concentration (SIC, filled contour) and 500 hPa geopotential height (GP500, black lines contour). Panel a shows correlation between ssNa$^+$ annual values and SIC and GP500 averaged over the period March, April, May, June, July, August, September, October and November (MAMJJASON) time series. Panel b shows correlation between ssNa$^+$ annual values and SIC and GP500 averaged over the period September, October and November (SON) time series. Panel c shows correlation between ssNa$^+$ annual values and SIC and GP500 averaged over the period June, July, August (JJA) time series. Green line represents Sea Ice
228 Concentration at 0.20 contour as proxy of seasonal Sea Ice extension limit.

229 The spatial correlation between smoothed ssNa$^+$ flux and Sea Ice Cover (SIC) and ECMWF era

230 Interim Geopotential Height at 500 hPa (GP), during March-November (MAMJJASON) are

231 highlighted in figure 3. Both SIC and GP fields are smoothed with a 3-year running average in

232 order to be consistent with smoothed ssNa$^+$ flux time series. The comparison with SIC shows

233 relative high correlation (figure 3a) in the Ross Sea, in the Western Pacific Sector and along Wilkes

234 Land at the boundaries of the sea ice edge where sea ice variability is greatest. On the other hand

11

235 strong anti-correlation appears in the Bellingshausen sea, along the Antarctic Peninsula coasts and

236 in the Weddell sea.
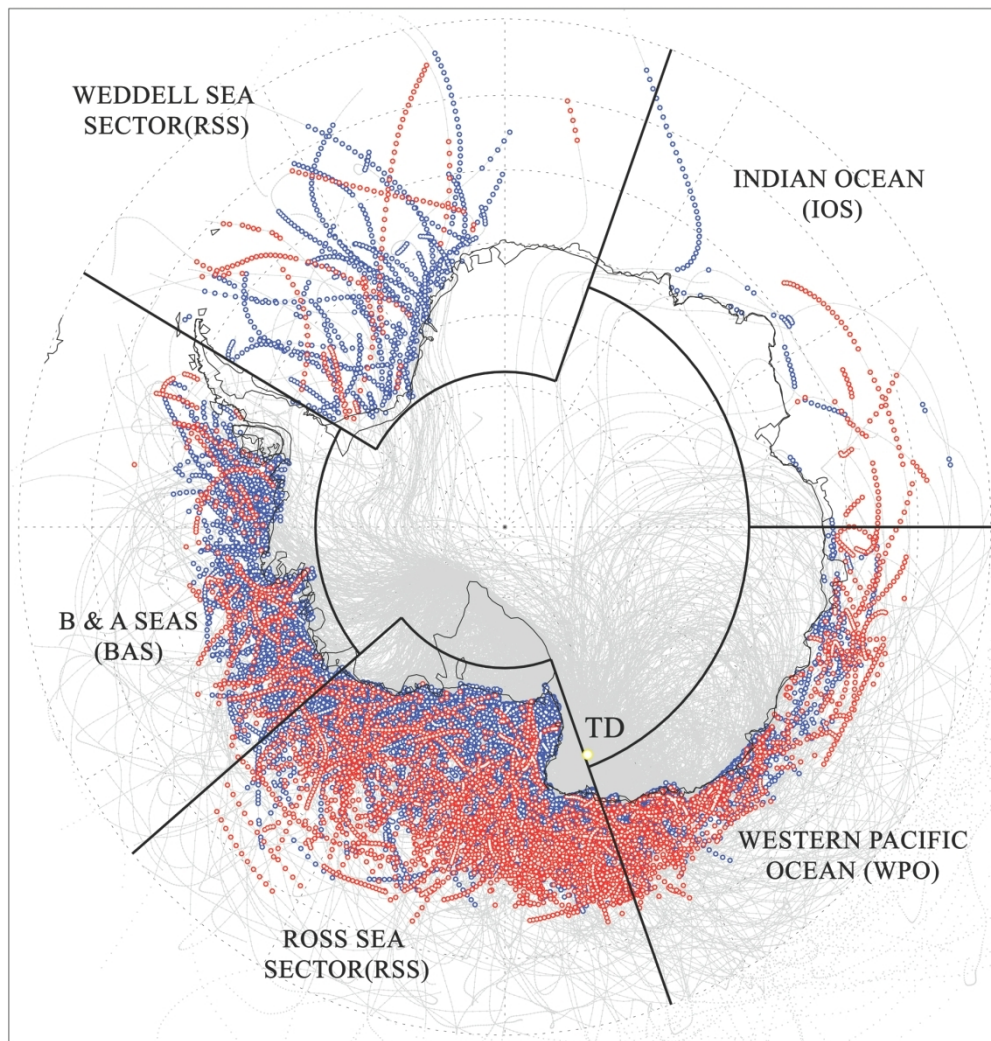
237

Figure 4. Three-day back-trajectories (TJ) for the period 1979-2003 arriving at 1000 m and 3000 m over TD at 12UTC (gray lines) generated using HYSPLIT model and related to possible ssNa$^+$ loads. Blue and Red points show where the selected TJs arriving at 1000 and 3000 m above TD, respectively, meet loading criteria (at least 3 points along the path where Sea Ice cover (SIC) > 0.50, 10 m Wind Speed (WS) > 5 m/s and 50 < TJ height < 500 m above the ground). Black lines highlight ocean sectors boundaries, Ross Sea (RSS), Western Pacific Ocean (WPO), Indian Ocean (IOS), B&A Seas (BAS) and Weddell Sea (WSS), as defined by Parkinson et al. (2012).

238

239   The correlation with the GP shows a large negative feature spread over East Antarctica and

240 extending to southern oceans and Ross Sea with a large minimum above Oates and Wilkes lands.

241 These correlations are enhanced during winter period (JJA, figure 3c) where most of SIC over Ross

242 Sea and Western Pacific seems positively correlated to Na$^+$ flux with maxima along the sea ice

12

243   edge. Particularly interesting is the JJA spatial correlation with GP which is no more elongated over

244   all the East Plateau but it is now concentrated over the Ross Sea sector with a centre of action above

245   the maximum correlation between Na^+ flux and SIC. These features are probably connected to the

246   increasing (decreasing) of storm track passage over Southern Ocean between 150° E and 150°W

247   and consequently decreasing (increasing) in pressure and geopotential fields and enhance (suppress)

248   of $ssNa^+$ advection to Talos Dome site.

249   In order to understand possible $ssNa^+$ path from source regions toward the TD site, we selected TJ

250   which show along their path at least three points where interpolated SIC and wind speed are greater

251   than 0.50 and 5 m/s , respectively, and the altitudes are comprised between 50 and 500 m above the

252   ground. The TJ analysis in figure 4 suggests that the provenance of air masses, possibly related to

253    $ssNa^+$ transport to TD, are mainly from the Western Pacific and Ross Sea sectors (130°W-130E°).

254   TJ ending at 1000 m above TD generally encounter favourable conditions for loading Na^+ close to

255   the Antarctic coasts of Oates, Victoria and Marie Byrd Lands and Ross Sea. On the other hand TJs

256   ending at 3000m above TD generally meet loading conditions off-shore, with loads prevalently over

257   Southern Ocean between 70° and 65°S close to the sea ice edge. The selected TJs are mainly

258   distributed over winter months and partly during the end of autumn and beginning of spring. Sala et

259   al (2008), using a similar analysis but with slightly different conditions, highlighted the same

260   loading areas with preferences of the Ross Sea sector during fall and spring and from the Southern

261   and Indian Ocean sectors during winter.

262   Spatial correlation and TJs analysis point out that formation and variability of the sea ice over the

263   entire Ross Sea and Western Pacific Ocean sectors, especially during winter months, could be

264   connected to $ssNa^+$ flux as measured at TD site. For this reason we selected the whole Ross Sea and

265   Western Pacific sectors as the most probable source areas of $ssNa^+$ and we investigated the role of

266    $ssNa^+$ at Talos Dome as a sea ice proxy.

267   Figure 5a shows the September SIE maxima from 1979 to 2003 as the sum of the Ross Sea and the

268   Western Pacific Ocean sectors September SIE maxima (dark red line) and the $ssNa^+$ annual mean

269   flux (dark green line) and their 3-year running average (black dotted lines) over the 25-year long

270   record. A general good agreement can be observed between the two series trends. The two main

271   peaks at the beginning and end of the profiles seem to be in phase whereas is not always true for the

272   smaller relative maxima in the middle of the records. Indeed, these 1-year shifts could be explained

273   by a possible dating error due to the relatively low accumulation rate at Talos Dome site, which can

274   be minimized by running averages but not completely excluded As already done by Iizuka et al.

275   (2008), we compared the yearly averaged log (ssNa$^+$ flux) with the time series of September SIE

276   maxima obtained from the sum of the Ross Sea and the Western Pacific Ocean both smoothed with

277   a 3-year running average (see figure 5b). The value of the Pearson's correlation coefficient (*r*) was

278   0.713, statistically significant at 1%. Significance was calculated using two-tail t-test with a

279   measure of effective degree of freedom as defined in Livezey and Chen (1983). The relationship

280   between the SIE and the log (ssNa$^+$ flux) can be described by a simple linear regression according

281   to this equation:

282   SIE maxima $_{\text{Ross Sea + Southern Indian Ocean}}$ (10^6 km^2) = 0.907 × log [ssNa$^+$ flux] (ng cm^{-2} a^{-1}) + 4.12 (Eq.

283   1)
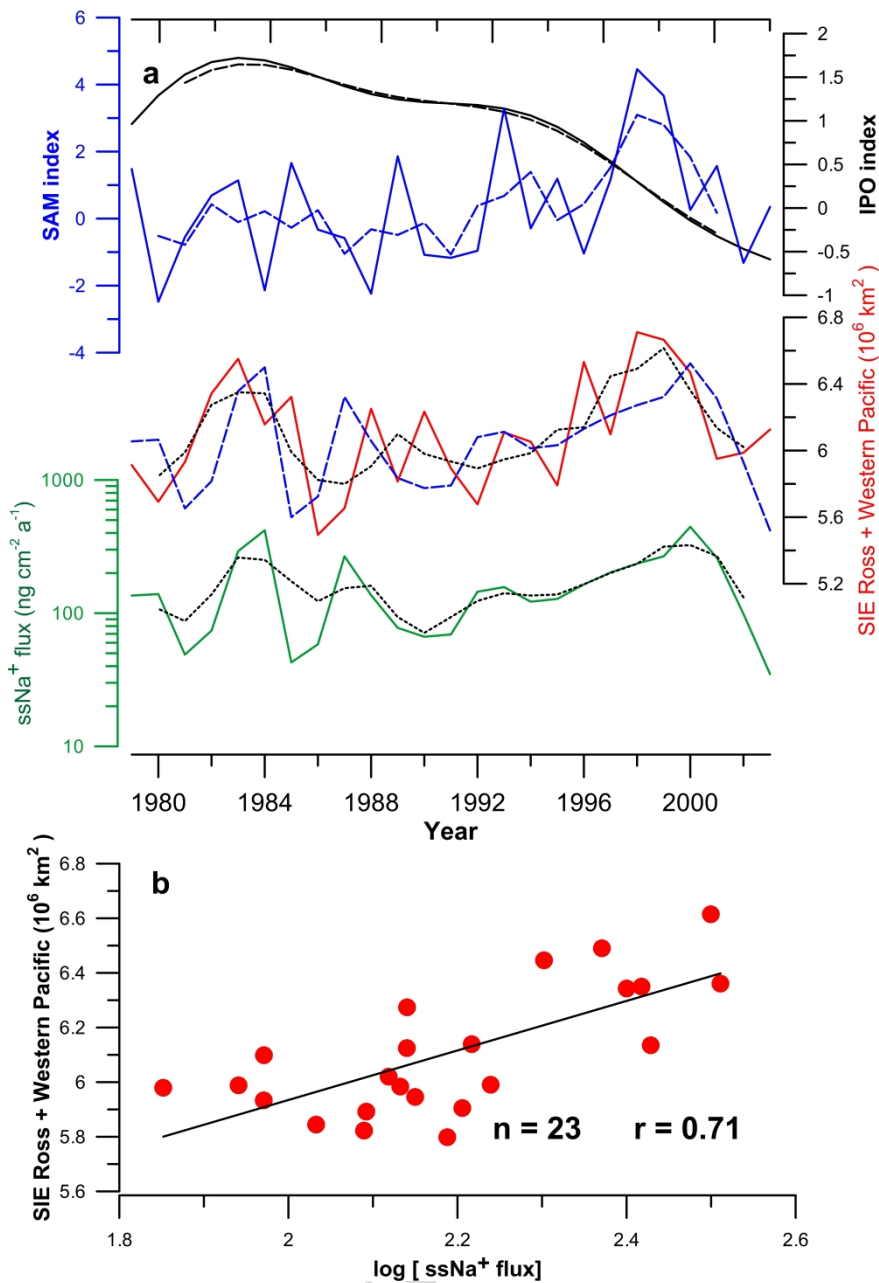
Figure 5. (a) Yearly average ssNa+ flux (in ng cm^{-2} a^{-1}) between 1979 and 2003 as measured in the Talos Dome snow pit (green line). For the same period the Sea Ice Extent as the sum of Ross Sea and Western Pacific Ocean (red line) and the reconstructed SIE (blue dashed line) are also shown. The solid black line and the solid blue line in the top panel represent the Southern Annular Mode (SAM) and Interdecadal Pacific Oscillation (IPO) indexes respectively. The corresponding dashed lines represent the 3-years running average. **(b)** Linear regression fit of the SIE (sum of September maxima of the Ross Sea and the Indian Ocean sectors) and log (ssNa$^+$ flux) for the time period ranging from 1979 to 2003. Pearson's *r* for the 23 data points used in the regression is 0.713.

284

285

286   According to Eq. (1) we used our yearly-averaged ssNa$^+$ fluxes in order to calculate a modeled SIE

287   maximum for each year in the time range between 1979 and 2003. The profile of this modelled Sea

15

288   Ice Extent is shown as a blue dashed line in figure 5a. We observe a general agreement between the

289   modelled and satellite-derived Sea Ice Extent, even if our simple linear model is not able to depict

290   short-term variations (e.g. the 1990 or 1996 SIE peaks are completely missing).

291   Moreover, we can assess that for log (ssNa$^+$ flux) values similar to the present ones, we can reliably

292   derive SIE maxima also in the past as already done at Talos Dome as a qualitative reconstruction by

293   Buiron et al. (2012) for a time period spanning between 20.000 and 50.000 years BP (before 1950

294   AD). We have to keep in mind that the SIE calibration shown in this paper might not continue in a

295   linear way beyond the range shown here.

296   The top panel of figure 5a shows the trends of the IPO and SAM indexes in the studied period,

297   highlighting a general agreement among these two indexes and our reconstructed SIE. Using the 3-

298   year averaged data for the IPO and SAM indexes (dashed lines in the top panel of figure 5a) and

299   calculating the Pearson's correlation coefficient we found that r = -0.44 (p<0.0001) and 0.61

300   (p<0.0001) respectively.

301   Meehl et al. (2016) showed how Antarctic sea ice expansion since 2000s has been driven by Pacific

302   decadal climate variability. Moreover several studies put in evidence the direct effect of IPO over

303   West Antarctica and Antarctic Peninsula temperatures and in atmospheric circulation across the

304   southern Pacific and Atlantic oceans. Conversely the IPO and ssNa$^+$ flux at TD site have similar

305   trends over inter-annual period but the relative low correlation seems to suggest no other direct

306   relationship.

307   On the other hand the teleconnection between SAM and ssNa$^+$ flux seems to be more pronounced.

308   The Annular mode has been shifted towards more positive state since 1950s (Thomson and

309   Solomon, 2002) with a deepening of the Amundsen Sea Low near Antarctica which caused a more

310   cyclone in the circumpolar through (Sinclair et al., 1997). This is consistent with the large spatial

311   anti-correlation between GP and Na$^+$ flux shown in figure 3c. The coupling of favorable atmosphere

312   dynamics and increase of surface where wind stress is able to blow up and transport toward coast

313   sea salt could be the possible link between sea ice and Na$^+$ flux at TD site.

314　Figure 6 shows the reconstruction of the September maximum SIE of the Ross Sea and Western

315　Pacific Ocean sectors achieved by using our TALDICE dataset and the modelled SIE from the

316　Ferrigno ice core (74°34'S, 86°54'W; Thomas and Abram, 2016) using MSA as a marker. The SIE

317　reconstruction by Curran et al. (2003) from the Law Dome ice core (66°46′S, 112°48′E) and the

318　Whitehall Glacier (72°54'S, 169°5'E; Sinclair et al., 2014) deuterium excess based SIE

319　reconstructions are shown in figure 6 as well.
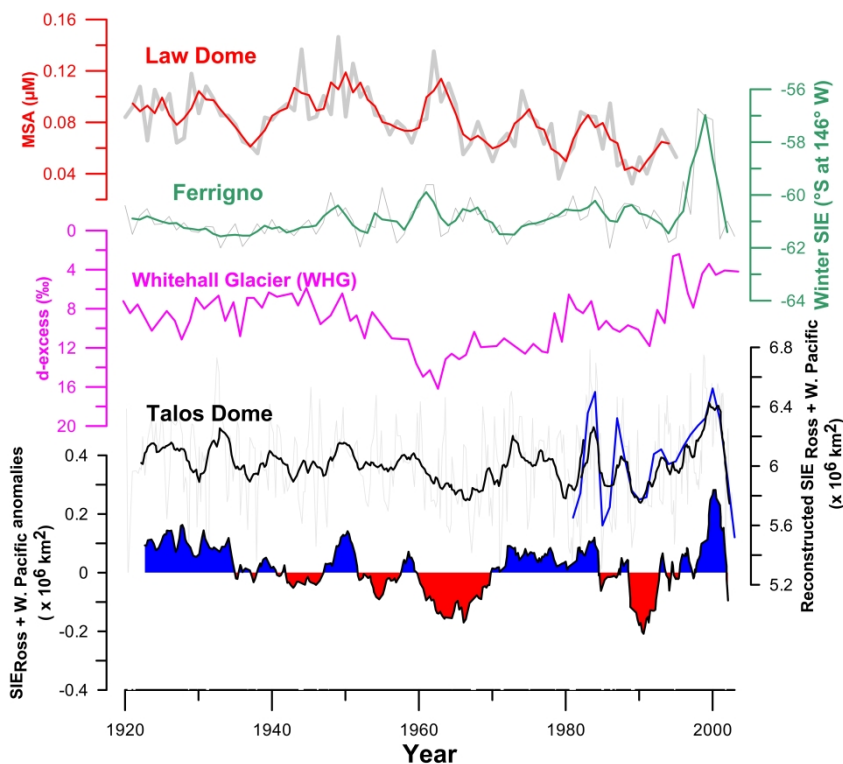
Figure 6. Reconstructed SIE as the sum of the Ross Sea and Pacific sectors of the Southern Ocean between 1920 and 2003. The black solid line shows the 13-points smoothed profile obtained using our Eq. (1) and the ssNa$^+$ flux measured in the TALDICE ice core and in the snow pit. sampled at Talos Dome (close to the TALDICE drilling site). The blue solid line shows the September SIE maxima as the sum of the Ross Sea and Pacific sectors of the Southern Ocean obtained by satellite measurements. The solid red line shows the 3-years running average of Law Dome MSA concentration as reported in Curran et al. (2003). The solid green line shows the 3-years running average of the SIE at 146°W as reconstructed by Thomas and Abram (2016). The solid magenta line shows the 3-year running average of the d-excess at WHG (rearranged from Sinclair et al., 2014). The bottom panel shows the SIE anomalies with respect to the 1920-2003 period.

323　In order to compare our SIE reconstruction with the previously published works, we have to keep in

324　mind that the three available ice core records used to reconstruct the past sea ice conditions, are

325　influenced by different sectors of the Southern Ocean. The Law Dome reconstruction refers to the

326　80°E-140°E sector, covering the Western Pacific Ocean and a small part of the Indian sector,

17

327 whereas at Ferrigno site MSA was found to depict the SIE across the Amundsen Ross sea, centred

328 on 146° W. The WHG record, based on d-excess and MSA, depicts the Ross Sea sea ice conditions,

329 overlapping the major part of our reconstructed area and for this reason represents the most

330 interesting site to compare with TD.

331 The smoothed profile of the SIE at TD in figure 6 (solid black line) shows rather stable winter sea

332 ice maxima over the 1920-1960 period. Since the 1960s the SIE anomalies of our reconstruction

333 with respect to the whole period (figure 6 - bottom panel) suggest an increased decadal-scale

334 variability in the recent decades with respect to the beginning of the century as already found by

335 Thomas and Abram (2016) in the Amundsen-Ross sea sector Furthermore, the reconstructed profile

336 of the SIE in the Ross Sea and Western Pacific Ocean sectors highlights that SIE during the late

337 1990s was the greatest of the whole century, as observed in reconstructions by Thomas and Abram

338 (2016) and Sinclair et al. (2014); during the late 90s we can in fact observe the highest positive SIE

339 anomalies over the last century (see bottom panel of figure 6).

340 The Law Dome record shows a continuous decline in the SIE starting from the 1950s and lasting to

341 the end of the record; the onset of this decreasing trend in SIE is also visible in the Ross Sea sector

342 as recorded in the TD and WHG reconstruction whereas it is not observed in the Ferrigno record.

343 Despite the almost coeval beginning of this decreasing trend for TD, Law Dome and WHG

344 reconstructions, we can observe an inversion in the SIE decline in the TD and WHG records

345 starting from the late 1990s, when we have previously noticed the beginning of a negative phase of

346 the IPO, whereas this inversion of trend is not visible in the Law Dome record.

347

348 **4. Conclusions**

349 We showed in this work that ssNa$^+$ flux in the Talos Dome region during a 25-year period spanning

350 from 1979 to 2003 is consistent with the idea of using it as a proxy for reconstructing the Sea Ice

351 Extension in the Ross Sea and Western Pacific Ocean, at least for recent decades. We found a

352 statistically significant positive linear relationship between the log (ssNa$^+$ flux) and the SIE

353 calculated by satellite data and through this relationship we were able to reconstruct the SIE profile

354 directly from our ssNa$^+$ data for a 25-year long period. Therefore, we used this positive relationship,

355 along with an assumption that the relationship is stationary, to reconstruct past SIE fluctuation for

356 the 20th century, pointing out a higher variability of SIE from the 1960s. Moreover, we found that

357 the last two decades show the highest SIE during the last century as already observed by other

358 records. Using our approach, ssNa$^+$ could prove to be a proxy for SIE in this area, allowing to

359 achieve a very high temporal resolution history of its past fluctuations for the last thousands years.

360 Although our findings strongly support a relationship between ssNa$^+$ and SIE, it is also clear that

361 meteorological conditions responsible for uplift and transport of sea-salt aerosol from the sea ice

362 surface to the ice sheet have a strong influence on the ssNa$^+$ flux. Current and future efforts in sea

363 salt aerosol modeling will improve the understanding of the information hidden in the ssNa$^+$ ice

364 core records.

365

377

378 **References**

19

379 Abram, N.J., Thomas, E.R., McConnell, J.R., Mulvaney, R., Bracegirdle, T.J., Sime, L.C.,

380 Aristarain, A.J., 2010. Ice core evidence for a 20th century decline of sea ice in the Bellingshausen

381 Sea, Antarctica. Journal of Geophysical Research-Atmospheres 115, D23101.

382 http://dx.doi.org/10.1029/2010JD014644.

383 Abram, N. J., Mulvaney, R., and Arrowsmith, C. 2011. Environmental signals in a highly resolved

384 ice   ore   from   James   Ross   Island,   Antarctica,   J.   Geophys.   Res.,   116,   D20116,

385 doi:10.1029/2011jd016147.

386 Abram, N. J., E. W. Wolff, and M. A. J. Curran , 2013. A review of sea ice proxy information from

387 polar ice cores, Quat. Sci. Rev., 79, doi:10.1016/j.quascirev.2013.01.011.

388 Allen, C.S., Pike, J., Pudsey, C.J., 2011. Last glacial-interglacial sea-ice cover in the SW Atlantic

389 and its potential role in global deglaciation. Quat. Sci. Rev. 30, 2446-2458.

390 Armand, L.K., Crosta, X., Romero, O., Pichon, J.J., 2005. The biogeography of major diatom taxa

391 in Southern Ocean sediments: 1. Sea ice related species. Palaeogeogr. Palaeoclimatol. Palaeoecol.

392 223 (1–2), 93–126.

393 Armand, L.K., Crosta, X., Queguiner, B., Mosseri, J., Garcia, N., 2008. Diatoms preserved in

394 surface sediments of the northeastern Kerguelen Plateau. Deep- Sea Res. Part II 55 (5–7), 677–692.

395 Baldwin, M. P., 2001: Annular modes in global daily surface pressure. Geophys. Res. Lett., 28,

396 4115–4118.

397 Bazin, L., Landais, A., Lemieux-Dudon, B., Toyé Mahamadou Kele, H., Veres, D., Parrenin, F.,

398 Martinerie, P., Ritz, C., Capron, E., Lipenkov, V., Loutre, M.-F., Raynaud, D., Vinther, B.,

399 Svensson, A., Rasmussen, S. O., Severi, M., Blunier, T., Leuenberger, M., Fischer, H., Masson-

400 Delmotte, V., Chappellaz, J., and Wolff, E.: An optimized multi-proxy, multi-site Antarctic ice and

401 gas orbital chronology (AICC2012): 120–800 ka, Clim. Past, 9, 1715– 1731, doi:10.5194/cp-9-

402 1715-2013, 2013.

403 Becagli, S.; Proposito, M.; Benassai, S.; Flora, O.; Genoni, L.; Gragnani, R.; Largiuni, O.; Pili, S.;

404 Severi, M.; Stenni, B.; Traversi, R.; Udisti, R.; Frezzotti, M. Chemical and isotopic snow variability

405 in East Antarctica along the 2001/02 ITASE traverse. Ann. Glaciol. 2004, 39, 473−482.

406 Becagli, S., Castellano, E., Cerri, O., Curran, M., Frezzotti, M., Marino, F., Morganti, A., Proposito,

407 M., Severi, M., Traversi, R., Udisti, R., 2009. Methanesulphonic acid (MSA) stratigraphy from a

408 Talos Dome ice core as a tool in depicting sea ice changes and southern atmospheric circulation

409 over the previous 140 years. Atmospheric Environment 43, 5, 1051-1058. http://dx.doi.org/10.1016/

410 j.atmosenv.2008.11.015.

411 Becagli S., Lazzara L., Marchese C., Dayan U., Ascanius S.E., Cacciani M., Caiazzo, L. Di Biagio

412 C., Di Iorio T., di Sarra A., Eriksen P., Fani F., Giardi, F. Meloni D., Muscari G., Pace G., Severi

413 M., Traversi R., Udisti. R., 2016. Relationships linking primary production, sea ice melting, and

414 biogenic aerosol in the Arctic. Atm. Env., 136, 1-15, doi:10.1016/j.atmosenv.2016.04.002.

415 Belt, S.T., Masse, G., Rowland, S.J., Poulin, M., Michel, C., LeBlanc, B., 2007. A novel chemical

416 fossil of palaeo sea ice: IP25. Organic Geochemistry 38, 16-27.

417 Belt, S.T., Müller, J., 2013. The Arctic sea ice biomarker IP25: A review of current understanding

418 and recommendations for future directions. Quaternary Science Reviews 79, 9-25.

419 Bopp, L., Kohfeld, K.E., Le Quéré, C., 2003. Dust impact on marine biota and atmospheric CO2

420 during glacial periods. Paleoceanography 18 (2).

421 Bowen, H.J.M., 1979. Environmental Chemistry of the Elements. Academic Press, London.

422 Brandt, R.E., Warren, S.G., Worby, A.P., Grenfell, T.C., 2005. Surface albedo of the Antarctic sea

423 ice zone. Journal of Climate 18 (17), 3606-3622.

424 Buiron, D., Stenni, B., Chappellaz, J., Landais, A., Baumgartner, M., Bonazza, M., Capron, E.,

425 Frezzotti, M., Kageyama, M., Lemieux-Dudon, B., Masson-Delmotte, V., Parrenin, F., Schilt, A.,

426 Selmo, E., Severi, M., Swingedouw, D., Udisti, R., 2012. Regional imprints of millennial variability

427 during the MIS 3 period around Antarctica. Quat. Sci. Rev. 48, 99-112.

428 Caiazzo L., Becagli S., Frosini D., Giardi F., Severi M., Traversi R., Udisti R., 2016. Spatial and

429 temporal variability of snow chemical composition and accumulation rate at Talos Dome site (East

430 Antarctica). Sci. Tot. Env. 550, 418–430.

431 Cavalieri, D.J., Parkinson, C.L., 2008. Antarctic sea ice variability and trends, 1979-2006. Journal

432 of Geophysical Research-oceans 113 (C7), C07004. http://dx.doi.org/10.1029/2007jc004564.

433 Collins, L. G., C. S. Allen, J. Pike, D. A. Hodgson, K. Weckström, and G. Massé (2013).

434 Evaluating highly branched isoprenoid (HBI) biomarkers as a novel Antarctic sea-ice proxy in deep

435 ocean glacial age sediments, Quat. Sci. Rev., 79, 87–98.

436 Criscitiello, A.S., Das, S.B., Evans, M.J., Frey, K.E., Conway, H., Joughin, I., Medley, B., Steig,

437 E.J., 2013. Ice-sheet record of recent sea-ice behaviour and polynya variability in the Amundsen

438 Sea, West Antarctica. Journal of Geophysical Research 118, 1-13.

439 http://dx.doi.org/10.1029/2012JC008077.

440 Curran, M. A. J., Van Ommen, T. D., and Morgan, V. 1998. Seasonal characteristics of the major

441 ions in the high-accumulation Dome Summit South ice core, Law Dome, Antarctica, Ann. Glaciol.,

442 27, 385–390.

443 Curran, M. A. J., van Ommen, T. D., Morgan, V. I., Phillips, K. L., and Palmer, A. S., 2003. Ice

444 Core Evidence for Antarctic Sea Ice Decline Since the 1950s, Science, 302, 1203–1206.

445 Dieckmann, G.S., Hellmer, H.H., 2010. The importance of sea ice: an overview. In: Thomas, D.N.,

446 Dieckmann, G.S. (Eds.), Sea Ice, second ed. Wiley-Blackwell, Oxford, 1-22.

447 Draxler, R.R., and G. D. Rolph, 2012. HYSPLIT (HYbrid Single-particle Lagrangian Integrated

448 Trajectory). NOAA Air Resources Laboratory, Silver Spring, MD. Model access via NOAA ARL

449 READY. Website. http://ready.arl.noaa.gov/HYSPLIT.php

450 Esper, O., Gersonde, R., 2014. New tools for the reconstruction of Pleistocene Antarctic sea ice.

451 Palaeogeogr. Palaeoclimatol. Palaeoecol. 399, 260-283.

452 http://dx.doi.org/10.1016/j.palaeo.2014.01.019.

453   Frezzotti, M., Urbini, S., Proposito, M., Scarchilli, C., Gandolfi, S., 2007. Spatial and temporal

454   variability of surface mass balance near Talos Dome, East Antarctica. J. Geophys. Res. 112

455   (F02032). doi:10.1029/2006JF000638.

456   Foster, A.F.M., Curran, M.A.J., Smith, B.T., van Ommen, T.D., Morgan, V.I., 2006. Covariation of

457   sea ice and methanesulphonic acid in Wilhelm II Land, East Antarctica. Annals of Glaciology 44,

458   429-432.

459   Gersonde, R., Crosta, X., Abelmann, A., Armand, L., 2005. Sea-surface temperature and sea ice

460   distribution of the Southern Ocean at the EPILOG Last Glacial Maximum − a circum-Antarctic

461   view based on siliceous microfossil records. Quat. Sci. Rev. 24 (7–9), 869–896.

462   Iizuka, Y., Hondoh, T., Fujii, Y., 2008. Antarctic sea ice extent during the Holocene reconstructed

463   from inland ice core evidence. Journal of Geophysical Research-Atmospheres, 113 (D15), D15114.

464   http://dx.doi.org/10.1029/2007jd009326.

465   Jones, J. M., S. T. Gille, H. Goosse, N. J. Abram, P. O. Canziani, D. J. Charman, K. R. Clem, X.

466   Crosta, C. de Lavergne, I. Eisenman, M. H. England, R. L. Fogt, L. M. Frankcombe, G. J. Marshall,

467   V. Masson-Delmotte, A. K. Morrison, A. J. Orsi, M. N. Raphael, J. A. Renwick, D. P. Schneider,

468   G. R. Simp-kins, E. J. Steig, B. Stenni, D. Swingedouw, and T. R. Vance, 2016. Assessing recent

469   trends in high-latitude Southern Hemisphere surface climate. Nat. Clim. Chang., 6, 917−926.

470   Levine, J. G., X. Yang, A. E. Jones, and E. W. Wolff, 2014. Sea salt as an ice core proxy for past

471   sea ice extent: A process-based model study, J. Geophys. Res. Atmos., 119,

472   doi:10.1002/2013JD020925.

473   Livezey, R. E., and W. Chen, 1983. Statistical field significance and its determination by Monte

474   Carlo techniques. Mon. Wea. Rev., 111, 46–59, doi: 10.1175/1520-0493(1983)111

475   Marshall, G. J., 2003. Trends in the Southern Annular Mode from observations and reanalyses. J.

476   Clim., 16, 4134-4143.

477 Massé, G., S. T. Belt, X. Crosta, S. Schmidt, I. Snape, D. N. Thomas, and S. J. Rowland, 2011.

478 Highly branched isoprenoids as proxies for variable sea ice conditions in the Southern Ocean,

479 Antarct. Sci., 23(05), 487–498.

480 Meehl, G.A., Hu, A., Santer, B.D., Xie, S.-P, 2016. Contribution of the Interdecadal Pacific

481 Oscillation to twentieth-century global surface temperature trends. Nat. Clim. Change, 6 (11),.1005-

482 1008, doi: 10.1038/nclimate3107.

483 Morganti, A., Becagli, S., Castellano, E., Severi, M., Traversi, R., Udisti, R., 2007. An improved

484 flow analysis—ion chromatography method for determination of cationic and anionic species at

485 trace levels in Antarctic ice cores. Anal. Chim. Acta 603, 190–198.

486 Parkinson, C. L., and D. J. Cavalieri, 2012. Antarctic sea ice variability and trends, 1979-2010. The

487 Cryosphere, 6, 871-880, doi:10.5194/tc-6-871-2012.

488 Rankin, A. M., Auld, V., and Wolff, E.W. 2000. Frost flowers as a source of fractionated sea salt

489 aerosol in the polar regions, Geophys. Res. Lett., 27, 3469–3472.

490 Roscoe, H. K., Brooks, B., Jackson, A. V., Smith, M. H., Walker, S. J., Obbard, R. W., and Wolff,

491 E. W. 2011. Frost flowers in the laboratory: growth, characteristics, aerosol, and the underlying sea

492 ice, J. Geophys. Res.-Atmos., 116, D12301, doi:10.1029/2010jd015144.

493 Röthlisberger, R., Mulvaney, R., Wolff, E.W., Hutterli, M.A., Bigler, M., Sommer, S., Jouzel, J.,

494 2002. Dust and sea salt variability in central East Antarctica (Dome C) over the last 45 kyrs and its

495 implications for southern high-latitude climate. Geophys. Res. Lett. 29 (20).

496 doi:10.1029/2002GL015186.

497 Sala, M., Delmonte, B., Frezzotti, M., Proposito, M., Scarchilli, C., Maggi, V., Artioli, G.,

498 Dapiaggi, M., Marino, F., Ricci, P. C., and De Giudici, G., 2008. Evidence of calcium carbonates in

499 coastal (Talos Dome and Ross Sea area) East Antarctica snow and firn: Environmental and climatic

500 implications, Earth. Planet. Sc. Lett., 271, 43–52, 2008.

501 Salinger, M.J., Renwick, J.A. and Mullan, A.B., 2001. Interdecadal Pacific Oscillation and South

502 Pacific climate. Int. J. Climatol., 21: 1705–1721. doi:10.1002/joc.691

503   Sarmiento, J.L., Gruber, N., 2006. Ocean Biogeochemical Dynamics. Princeton University Press,

504   Princeton.

505   Scarchilli, C., Frezzotti, M., and Ruti, P., 2011. Snow precipitation at four ice core sites in East

506   Antarctica: provenance, seasonality and blocking factors, Clim. Dyn., 37, 2107-2125,

507   10.1007/s00382-010-0946-4.

508   Schlosser, E., H. Oerter, V. Masson-Delmotte, and C. Reijmer, C., 2008. Atmospheric influence on

509   the deuterium excess signal in polar firn: Implications for ice-core interpretation. J. Glaciol., 54

510   (184), 117-124. http://dx.doi.org/ 10.3189/002214308784408991.

511   Serreze, M.C., Barry, R.G., 2011. Processes and impacts of Arctic amplification: a research

512   synthesis. Global and Planetary Change, 77 (1-2), 85-96. http://dx.doi.org/10.1016/j.gloplacha.

513   2011.03.004.

514   Severi, M., Becagli, S., Castellano, E., Morganti, A., Traversi, R., Udisti, R., 2009. Thirty years of

515   snow deposition at Talos Dome (Northern Victoria Land, East Antarctica): chemical profiles and

516   climatic implications. Microchem. J. 92, 15–20.

517   Severi, M., Udisti, R., Becagli, S., Stenni, B., and Traversi, R., 2012. Volcanic synchronisation of

518   the EPICA-DC and TALDICE ice cores for the last 42 kyr BP, Clim. Past, 8, 509–517,

519   doi:10.5194/cp-8-509-2012.

520   Simmons, A, S. Uppala, D. Dee, and S. Kobayashi, 2006, ERA-Interim: new ECMWF re-analysis

521   products from 1989 onwards., ECMWF Newslett, 110:25–35.

522   Sinclair, M.R., J.A. Renwick, and J.W. Kidson, 1997. Low-frequency variability of Southern

523   Hemisphere sea level pressure and weather system activity. Mon. Weather Rev., 125, 2531–2543.

524   Sinclair, K. E., N. A. N. Bertler,M.M. Bowen, and K. R. Arrigo, 2014. Twentieth century sea-ice

525   trends in the Ross Sea from a high-resolution, coastal ice-core record, Geophys. Res. Lett., 41,

526   3510–3516, doi:10.1002/2014GL059821.

527   Smith, B.T., van Ommen, T., Curran, M.A.J., 2004. Methanesulphonic acid movement in solid ice

528   cores. Annals of Glaciology 39, 540-544.

529 Spolaor, A., Vallelonga, P., Plane, J. M. C., Kehrwald, N., Gabrieli, J., Varin, C., Turetta, C., Cozzi,

530 G., Kumar, R., Boutron, C., and Barbante, C. 2013. Halogen species record Antarctic sea ice extent

531 over glacial-interglacial periods, Atmos. Chem. Phys., 13, 6623-6635, doi: 10.5194/acp-13-6623-

532 2013.

533 Spolaor, A., Vallelonga, P., Turetta, C., Maffezzoli, N., Cozzi, G., Gabrieli, J., Barbante, C., Goto-

534 Azuma, K., Saiz-Lopez, A., Cuevas, C. A., Dahl-Jensen, D., 2016. Canadian Arctic sea ice

535 reconstructed from bromine in the Greenland NEEM ice core. Sci. Rep. 6, 33925; doi:

536 10.1038/srep33925.

537 Stenni, B., Buiron, D., Frezzotti, M., Albani, S., Barbante, C., Bard, E., Barnola, J.M., Baroni,M.,

538 Baumgartner, M., Bonazza, M., Capron, E., Castellano, E., Chappellaz, J., Delmonte, B., Falourd,

539 S., Genoni, L., Iacumin, P., Jouzel, J., Kipfstuhl, S., Landais, A., Lemieux-Dudon, B., Maggi, V.,

540 Masson-Delmotte, V., Mazzola, C., Minster, B., Montagnat, M., Mulvaney, R., Narcisi, B., Oerter,

541 H., Parrenin, F., Petit, J.R., Ritz, C., Scarchilli, C., Schilt, A., Schüpbach, S., Schwander, J., Selmo,

542 E., Severi, M., Stocker, T.F., Udisti, R., 2011. Expression of the bipolar seesaw in Antarctic climate

543 records during the last deglaciation. Nat. Geosci. 4, 46–49.

544 Thomas, E. R., and N. J. Abram, 2016. Ice core reconstruction of sea ice change in the Amundsen-

545 Ross Seas since 1702 A.D., Geophys. Res. Lett., 43, 5309–5317, doi:10.1002/2016GL068130.

546 Thompson, D. W. J., and J. M. Wallace, 2000. Annular modes in the extratropical circulation, part

547 1, Month-to-month variability, J. Clim., 13, 1000– 1016.

548 Traversi, R.; Becagli, S.; Castellano, E.; Larguini, O.; Migliori, A.; Severi, M.; Frezzotti, M.;

549 Udisti, R., 2004. Spatial and temporal distribution of environmental markers from coastal to plateau

550 areas in Antarctica by firn core chemical analysis. Int. J. Environ. Anal. Chem., 84 (6−7), 457−470.

551 Vallelonga, P., Maffezzoli, N., Moy, A. D., Curran, M. A. J., Vance, T. R., Edwards, R., Hughes,

552 G., Barker, E., Spreen, G., Saiz-Lopez, A., Corella, J. P., Cuevas, C. A., and Spolaor, A., 2016. Sea

553 ice-related halogen enrichment at Law Dome, coastal East Antarctica, Clim. Past Discuss.,

554 doi:10.5194/cp-2016-74.

555   Veres, D., Bazin, L., Landais, A., Toyé Mahamadou Kele, H., Lemieux-Dudon, B., Parrenin, F.,

556   Martinerie, P., Blayo, E., Blunier, T., Capron, E., Chappellaz, J., Rasmussen, S. O., Severi, M.,

557   Svensson, A., Vinther, B., and Wolff, E. W.: The Antarctic ice core chronology (AICC2012): an

558   optimized multi-parameter and multi-site dating approach for the last 120 thousand years, Clim.

559   Past, 9, 1733–1748, doi:10.5194/cp-9-1733-2013, 2013.

560   Wolff, E., Fischer, H., Fundel, F., Ruth, U., Twarloh, B., Littot, G. C., Mulvaney, R., Rothlisberger,

561   R., de Angelis, M., Boutron, C. F., Hansson, M., Jonsell, U., Hutterli, M. A., Lambert, F.,

562   Kaufmann, P., Stauffer, B., Stocker, T. F., Steffensen, J. P., Bigler, M., Siggaard-Andersen, M. L.,

563   Udisti, R., Becagli, S., Castellano, E., Severi, M., Wagenbach, D., Barbante, C., Gabrielli, P., and

564   Gaspari, V. 2006. Southern Ocean sea-ice extent, productivity and iron flux over the past eight

565   glacial cycles, Nature, 440, 491–496.

566   Yang, X., Pyle, J.A., Cox, R.A., 2008. Sea salt aerosol production and bromine release: role of

567   snow   on   sea   ice.   Geophysical   Research   Letters   35   (16),   L16815.   http://

568   dx.doi.org/10.1029/2008gl034536.

SIE$_{Ross}$ + W. Pacific anomalies
(x 10^6 km^2)

Year

Reconstructed SIE$_{Ross}$ + W. Pacific
(x 10^6 km^2)